Front. Struct. Civ. Eng. 2022, 16(11): 1474–1485
https://doi.org/10.1007/s11709-022-0869-2

RESEARCH ARTICLE

Laboratory investigation of emulsified asphalt binder modified with wood-derived nano-cellulose and nano paper-cellulose

Yunge WEI, Jiayu WANG*, Ruoyu LI, Ling XU, Feipeng XIAO

Key Laboratory of Road and Traffic Engineering of Ministry of Education, Tongji University, Shanghai 200092, China
**Corresponding author. E-mail: jiayuwang@tongji.edu.cn*

ABSTRACT Emulsified asphalt is the primary material for preventive maintenance and cold-mix paving, but its low cohesive strength and poor mechanical properties limit its wide application, even with polymer modification. In this study, Styrene-Butadiene Rubber (SBR) emulsified asphalt was modified with nano-cellulose materials, namely nano paper-cellulose (NPC) and wood-derived nano-cellulose (WDC), to improve its properties. A novel preparation method of nano-cellulose solution was developed, including blending, ultrasonic stirring, and centrifugal treatment. Four types of nano-cellulose solution (0.5% NPC, 0.5%, 1.0%, and 1.5% WDC by weight of water) were selected. The microscopy analysis indicated that 0.5% WDC emulsion had a smaller particle size than 1.5% WDC emulsion. The rheology test indicated that WDC modified residue improved rutting resistance with the increased solution dosage due to the cross-linking effect, but its creep-and-recovery performance was worse than that of SBR emulsion residue. The NPC modified binder had a higher rutting factor than WDC modified binder at the same dosage after short-term aging. In addition, 1.0% WDC could be regarded as the optimal dosage in terms of fatigue and low-temperature performance. Furthermore, Fourier Transform Infrared Spectroscopy (FTIR) results showed that 0.5% NPC modified residue performed better in long-term aging resistance compared with 0.5%WDC modified asphalt.

KEYWORDS nano-cellulose, emulsified asphalt binder, dispersion, rheological properties, Fourier transform infrared spectroscopy

1 Introduction

Maintenance and rehabilitation projects with low-energy consumption and low greenhouse gas emissions (GHG) benefit the sustainable pavement system. Emulsified asphalt binder is a continuous water dispersion system of fine asphalt droplets, mainly composed of 40 wt.%–80 wt.% of asphalt binder, water, emulsifier, and stabilizer [1]. Emulsified asphalt binders are commonly used in pavement preservation techniques such as tack coat, fog seals, chip seals, and micro-surfacing. Asphalt emulsions are also well used for cold mix asphalt, cold in-place recycling, and stabilization because they can be mixed with aggregate at the ambient temperature to increase strength, effectively reducing the aging effect and energy consumption [2,3].

Styrene-Butadiene-Rubber (SBR) modified asphalt emulsion is widely used in cold mix asphalt due to its high bond strength with aggregate [1]. However, the poor rutting resistance of SBR emulsified asphalt mixture limits its use in high-temperature areas and heavy traffic loading pavements [4]. In addition, SBR emulsion is subject to adhesion loss and spalling failure when applied as a fog seal due to its low mechanical strength and low cracking resistance [5,6]. Numerous studies have been conducted to improve the performance of SBR modified asphalt emulsion, among which nanomaterials have been considered as suitable modifiers [7,8]. Nanomaterial is defined as a material with at least one dimension within the range from 1 to 100 nm [9]. Due to their small size,

Article history: Received Oct 24, 2021; Accepted May 21, 2022

the material composed of nanoparticles has different properties from macroscopic material, such as surface and interface effects, small size effect, quantum size effect, and macroscopic quantum tunnelling effect [10,11]. It has been found that incorporating nanoparticles can significantly improve the pavement performance of asphalt binders. The nanoparticles mainly include nano-carbon, nano-SiO_2, nano-ZnO, nano-TiO_2, and nano-clay [11]. Researchers have found that the addition of nano-clay could enhance thermal aging resistance and heat resistance of SBR [12]; the introduction of nano-ZnO could enhance the shear deformation resistance and elastic behavior of SBR [13], and nano-ZnO had a better ultraviolet aging resistance on modified asphalt than nano-SiO_2 and nano-TiO_2 [14].

In addition, it can be noted that nano-celluloses and nano-fibers have high strength, high specific surface area, degradability, and excellent mechanical properties [15,16]. Khattak et al. [17] found that the addition of carbon nano-fibers could increase the rutting factor of asphalt binder by 47%, and fatigue life could be prolonged by 2–3 times. Moreover, carbon nano-fibers significantly increased the permanent deformation resistance of the asphalt mixture [18]. Ghabchi and Castro [19] found that incorporating cellulose nano-fibers resulted in an asphalt mix with higher resistance to rutting and cracking. Jin et al. [20] pointed out that adding palygorskite nano-fiber could enhance the water stability, high-temperature stability, and anti-rutting capacity of asphalt binder. It has been found by using scanning electron microscopy (SEM) [21] that carbon nano-fibers have good adhesion properties and show high connectivity in asphalt binder, forming a fiber network to inhibit the generation of cracks. Therefore, the application of nano-fibers is a sustainable solution to improve the mechanical properties of asphalt binders [19].

However, the poor dispersion uniformity due to the agglomeration of nanomaterial is a challenge for nanomaterial modification [22]. The large specific surface area of nano-cellulose can directly cause an increase in the interfacial contact area and interaction rate [23]. When nano-cellulose is added into asphalt binder, it agglomerates gradually because of a large specific surface area and high surface energy. Moreover, if nano-cellulose is added to asphalt binders with high viscosity, the electrostatic force and van der Waals force between the nanoparticles can easily result in formation of large particle clusters [10,24]. This phenomenon affects the modification effect of nano-cellulose and even negatively affects the properties of asphalt binders. Therefore, whether the nano-cellulose can be effectively dispersed or not has become one of the most important concerns for asphalt modification. Currently, most scholars adopt a high blending temperature and a high shear speed during the preparation process. The nanomaterials are gradually added into a heated asphalt binder, and then the shear mixer is used to blend for 50–60 min [7,25]. This process mainly relies on high-speed physical shearing to disperse nanomaterials, but it has a limited dispersion effect and consumes lots of energy.

In this study, a novel preparation method is proposed to fabricate two types of nano-cellulose modified asphalt emulsion. Microscopic observation and digital image analysis were conducted to determine the dispersion uniformity of asphalt emulsion. Furthermore, the high-temperature rutting resistance, low-temperature cracking resistance, fatigue resistance, and aging resistance of nano-celluloses modified asphalt emulsion residues were evaluated.

2 Materials and methods

2.1 Materials

2.1.1 Emulsified asphalt binder

SBR modified asphalt emulsion is widely used for pavement surface treatment, with great elastic performance [26]. SBR asphalt emulsion with 3 wt.% SBR latex was used as a control binder in this study. Two SBR asphalt emulsions named SBR I and SBR II were provided by two different local contractors. The basic properties of two control emulsions and their residue are summarized in Table 1.

2.1.2 Nano-celluloses

Two kinds of nano-celluloses, named nano paper-cellulose (NPC) and wood-derived nano-cellulose (WDC), were selected in this study due to their low cost and sustainability. The NPC was recycled from waste paper and prepared in the laboratory, and the WDC was provided by a local company. An optical microscope was used to measure the average length and diameter of particles of the nano additives in 1% NPC and 1% WDC solution. It can be seen from Fig. 1 that the average length of particles of NPC (72 nm) was much lower than that of WDC (156 nm). In addition, the average diameter of NPC and WDC particles was less than 100 nm; the average diameter of NPC (10.6 nm) was larger than that of WDC (7.8 nm).

2.2 Sample preparation

2.2.1 Preparation of wood-derived nano-cellulose solution

As shown in Fig. 2(a), the preparation process of the WDC solution was divided into four steps [29]: weighing, blending, ultrasonic stirring, and centrifugal treatment.

Table 1 Basic properties of SBR asphalt emulsion (JTG E20-2011, JTG F40-2004) [27,28]

emulsion properties	unit	measured values		requirement	method
		SBR I	SBR II		
demulsification rate	–	slow	quick	–	T 0658
particle charge	–	cationic (+)	cationic (+)	–	T 0653
surplus on sieve (1.18 mm)	%	0.06	0.06	≤0.1	T 0652
engler viscosity (25 °C)	–	13	17.6	2–30	T 0622
storage stability (5 d)	%	1.1	0.20	≤5	T 0655
residue by distillation residue	%	59	62.5	≥50	T 0651
softening point	°C	58.1	57.5	–	T 0606
penetration (25 °C)	0.1mm	58.8	62	45–150	T 0604
ductility (15 °C)	cm	42	42	≥40	T 0605

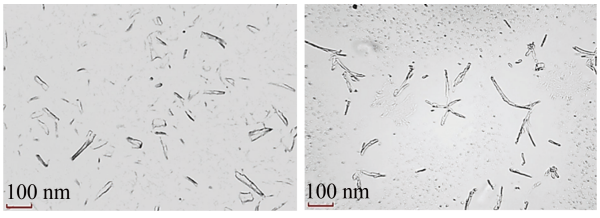

(a) (b)

Fig. 1 Optical microscope image of nano-cellulose solution. (a) 1% NPC solution; (b) 1% WDC solution.

First, 0.75, 1.5, and 2.25 g WDC were added into 150 mL distilled water, with continuous stirring. Then, the ultrasonic stirring device was used to disperse the cellulose for 15 min at 25 °C completely. After that, the suspension solution was centrifuged for 30 min at 8000 r·min^{-1}. Finally, the supernatant solution was obtained for further preparation.

2.2.2 Preparation of nano paper-cellulose solution

According to the method of A.P. Mathew et al. [30], pure NPC was extracted from raw wood by dilute acid hydrolysis in the bioethanol test device, then solvent extraction and bleaching were carried out and finally concentrated into water suspension, with a solid content of 17%, by centrifugation.

In this study, the sample preparation process had five steps, as shown in Fig. 2(b). The first step was to weigh 8 g of recycled paper, dissolve it into 100 mL deionized water, and mash it into small pieces using a blender. Next, the cellulose was oxidized by 2,2,6,6-tetramethyl-pyridine-1-oxy (TEMPO), sodium bromide and sodium hypochlorite in aqueous solution [31,32]. In this step, the cellulose was suspended in the solution containing TEMPO and sodium bromide. Sodium hypochlorite was added into the TEMPO mediated cellulose suspension at room temperature and a pH value of 10.5. After stirring the cellulose suspension for 5–6 h, the suspension gradually became a milky white material. Then, the suspension solution was centrifuged for 30 min at 8000 r·min^{-1} and stirred by ultrasonic devices for three times. Finally, the NPC was obtained by mashing the bottom cellulose after pouring out the supernatant.

2.2.3 Preparation of nano-cellulose emulsified asphalt binder

As shown in Fig. 2(c), three concentrations of WDC solutions (0.5 wt.% WDC, 1.0 wt.% WDC, and 1.5 wt.% WDC) and 0.5 wt.% NPC were prepared in this study. These four different nano-cellulose solutions were then added into SBR emulsified asphalt binder. The added nano-cellulose solution had the same mass as the SBR emulsified asphalt residue. After ultrasonic stirring and magnetic stirring treatment at room temperature (500 r·min^{-1}), the nano-cellulose modified asphalt binders were prepared as shown in Fig. 2(d). Then, the emulsified asphalt binder was heated at 163 °C until the moisture had completely evaporated according to JTG E20-T 0651. Finally, the residue of nano-cellulose modified asphalt binder was obtained.

2.3 Experiment methods

2.3.1 Micro-topography

For the particle size determination of emulsified asphalt binder, the asphalt emulsion was first diluted to 10–20 times by deionized water, and then the particle diameter was measured under 500× magnification by optical microscope. The digital image analysis was conducted to determine the particle size distribution of the emulsified asphalt binder.

2.3.2 Aging method

This study used the Rolling Thin Film Oven (RTFO) and

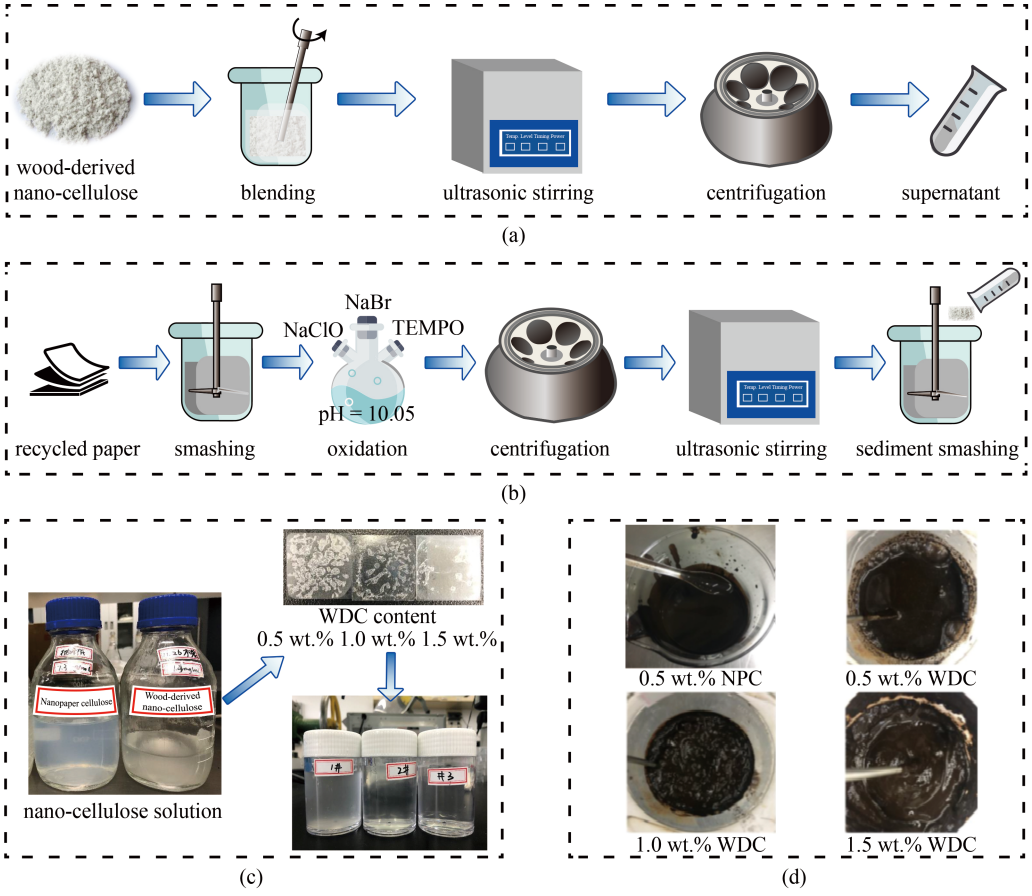

Fig. 2 The preparation process of nano-cellulose modified asphalt binders. (a) The preparation process of WDC solution; (b) the preparation process of NPC solution; (c) the photos of prepared nano-cellulose solutions and their residues; (d) the photos of nano-cellulose modified asphalt binders at various percentages.

Pressurized Aging Vessel (PAV) to simulate short-term aging and long-term aging, respectively. During the RTFO aging, the asphalt residue was heated at 163 °C for 85 minutes according to the JTG E20-2011 standard. The PAV aging tests were carried out at 100 °C and 2.1 MPa for 20 h.

2.3.3 Dynamic shear rheometer test

The complex shear modulus (G^*) and phase angle (δ) of the virgin, RTFO aged, and PAV aged asphalt binders were determined by dynamic shear rheometer (DSR) in oscillation mode according to AASHTO T 315 [33]. The rutting factors $G^*/\sin\delta$ of virgin and RTFO aged, and fatigue factor $G^*\cdot\sin\delta$ of PAV aged binders were calculated. Two replicate samples of each type of asphalt residue were tested.

The results from the high-temperature DSR test were used to evaluate the impact of nano-cellulose on the aging resistance of asphalt binder. The rutting factor aging index (RAI, %) was determined through Eq. (1).

$$RAI(\%) = \frac{(G^*\cdot\sin\delta)_{\text{aged}} - (G^*\cdot\sin\delta)_{\text{unaged}}}{(G^*\cdot\sin\delta)_{\text{unaged}}} \times 100\%. \quad (1)$$

The frequency sweep test was conducted at 64 °C from 0.01 to 20 Hz under shear stress of 0.1 kPa. These testing parameters were determined by amplitude sweep test to ensure the test remained in the linear viscoelastic region. In addition, the multiple stress creep and recovery test (MSCR) was conducted at 64 °C under stress levels of 0.1 and 3.2 kPa according to AASHTO T 350. During each test cycle, the sample was subjected to a constant stress for 1 s followed by a recovery period of 9 s. The non-recoverable creep compliance (J_{nr}) is the ratio of residual strain and stress of asphalt residues after creep and recovery cycles. The recovery percent (R) is the average ratio of recovered strain to maximum strain in every cycle. The lower J_{nr} and higher R indicate better high-temperature permanent deformation resistance under repeated load.

2.3.4 Bending beam rheometer test

The BBR test was used to determine the creep stiffness of asphalt binders versus loading time at low temperatures. In this study, the low-temperature performance of four emulsified asphalt residues after PAV aging was determined at three temperatures (–6, –12, and –18 °C)

based on AASHTO T350. Two replicate beams of each type of asphalt residue were tested and their average stiffness modulus (S) and creep rate (m) at 60 s were calculated. In addition, the indicator ΔT_c was introduced to evaluate the non-load-associated cracking resistance of asphalt residue [34]. The definition of ΔT_c is the difference between the critical temperatures determined by stiffness (S) and m-value at 60 s, as shown in Eq. (2). The former studies have recommended that the safety threshold of ΔT_c should be above –2.5 °C [35].

$$\Delta T_c = T_{C,S}(60\text{ s}) - T_{C,m}(60\text{ s}), \quad (2)$$

where $T_{C,S}$ and $T_{C,m}$ are the critical temperatures determined by stiffness (S) and m-value at 60 s, respectively.

2.3.5 ATR-FTIR test

In this study, the attenuated total reflection Fourier transform infrared spectroscopy (ATR-FTIR) was used to characterize the functional groups of nano-cellulose modified asphalt binders. The infrared spectra of samples ranged from 4000 to 600 cm^{-1} with a 4 cm^{-1} resolution. Three replicates were tested for each asphalt residue to reduce experimental error. In addition, the spectra obtained from the scans were analyzed through the OMNIC software to determine the aging effect of nano-cellulose modified asphalt binders. The chemical index of functional groups (S=O at 1030 cm^{-1} and C=O at 1735 cm^{-1}) were defined as the peak areas (CH_3 at 1375 and 1458 cm^{-1}) divided by the peak area of aging related functional group, as shown below [36].

$$I_{S=O} = \frac{\text{Peak area at 1030 cm}^{-1}}{\text{Peak areas at 1375 cm}^{-1}\text{ and 1458 cm}^{-1}}, \quad (3)$$

$$I_{C=O} = \frac{\text{Peak area at 1735 cm}^{-1}}{\text{Peak areas at 1375 cm}^{-1}\text{ and 1458 cm}^{-1}}. \quad (4)$$

3 Results and discussion

3.1 The effect of WDC content on emulsion particle size and distribution

The particle size and its distribution of emulsified asphalt binder significantly impact the strength of emulsified asphalt mixture [37] because the specific surface area of asphalt emulsion increases with decreasing particle size. The asphalt emulsion can uniformly disperse in the asphalt mixture and tightly coat with aggregate when the appropriate particle size is used. In this study, the particle size of nano-cellulose modified asphalt binder with different contents of WDC was measured by an optical microscope. Figures 3(a) and 3(b) show the microstructure of 0.5% WDC and 1.5% WDC modified emulsified asphalt binders at 500× magnification. The black spots in the images were asphalt particles which can be identified by digital image recognition software. The particle size and its distribution are summarized in Table 2.

Both average and maximum particle sizes of 0.5% WDC modified emulsified asphalt were lower than those of 1.5% WDC modified emulsified asphalt binder. In addition, all the particles of 0.5% WDC modified emulsified asphalt binder were smaller than 5 μm, while

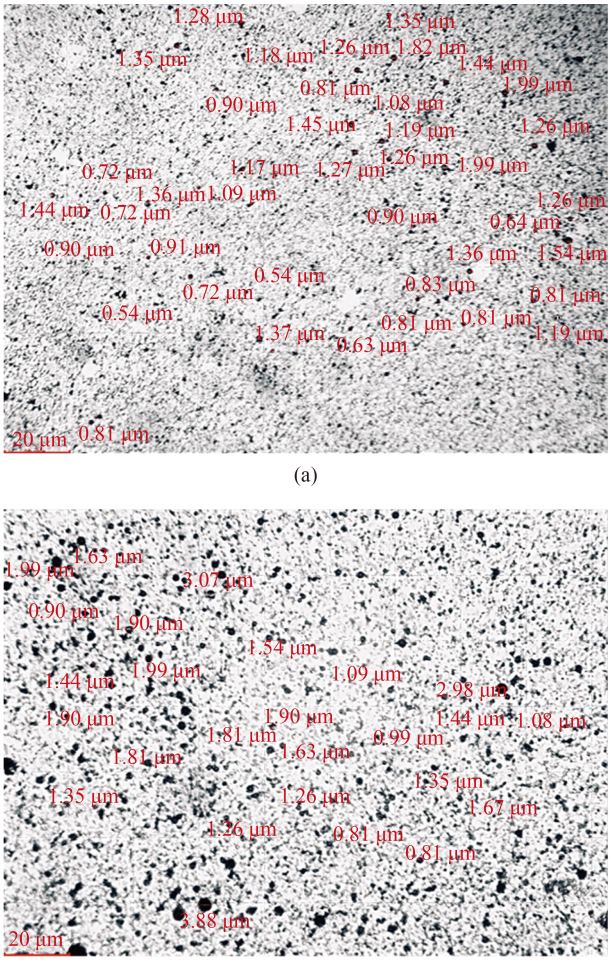

(a)

(b)

Fig. 3 The microscopy image of nano-cellulose modified emulsified asphalt binder under 500× magnification. (a) 0.5% WDC modified emulsified asphalt binder; (b) 1.5% WDC modified emulsified asphalt binder.

Table 2 WDC modified emulsified asphalt microscopic particles

emulsion type	average particle size (μm)	maximum particle size (μm)	5 μm	>10 μm
0.5% WDC emulsion	1.36	2.12	100%	–
1.5% WDC emulsion	2.61	5.28	90%	–

10% of particles in 1.5% WDC emulsified asphalt binder were between 5 and 10 μm. It could be inferred that with the increase of the content of nano cellulose, due to the -OH groups on the surface of nano-cellulose [38], nano-cellulose absorbed more moisture under the action of the hydrogen bond.

3.2 The effect of WDC content on rutting factor

Figure 4 shows the rutting factor ($G^*/\sin\delta$) of SBR II emulsion residues and WDC modified SBR II residues at a temperature range from 64 to 76 °C. As expected, the rutting factor of asphalt residue decreased rapidly with increased test temperatures. With the increase of WDC content (0.5%, 1.0%, and 1.5% of WDC), the rutting factor increased significantly regardless of test temperature. However, it can be noted that the rutting factor of 0.5% WDC modified binder was slightly higher than that of the control asphalt binder because nano-cellulose with less content cannot form a stable cross-linking in asphalt binder. In addition, WDC with poor heat resistance cannot effectively improve the high-temperature performance of asphalt. Therefore, the rutting factor reduced significantly with increased temperature, especially at high WDC content.

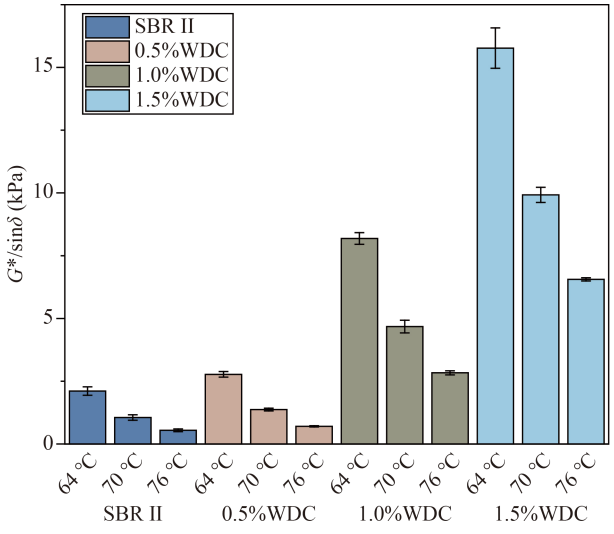

Fig. 4 $G^*/\sin\delta$ of various contents of WDC modified binder residues at 64 °C, 70 °C, and 76 °C.

3.3 The effect of WDC content on creep and recovery behavior

Figure 5 summarizes J_{nr} and $R\%$ for residues at the stress levels of 0.1 and 3.2 kPa. It can be found that the control binder had the best elastic behavior among tested residues because the addition of WDC broke the structure of SBR II latex to some extent. For example, the values of $R\%$ under 3.2 kPa of SBR II emulsion residue and 0.5% WDC emulsion residue were 21.2% and 0.9%, respectively. However, the $R\%$ of WDC emulsion residues increased from 0.9% to 12.8% with the increase of nano-cellulose content, indicating that the elastic properties of WDC emulsion residues improved. The J_{nr} of SBR II emulsion residue at 64 °C was 1.19 kPa^{-1}. This value doubled after adding 0.5% WDC, then gradually reduced to 0.58 kPa^{-1} with the addition of 1.5% WDC. A similar trend can also be found at 0.1 kPa. Therefore, test results indicated that 1.5% WDC had a positive effect on non-recoverable creep compliance or modulus of control binder but had no effect on recovery percentage due to the stiffness of the WDC network structure.

3.4 The effect of WDC content on frequency sweep

The frequency sweep results are shown in Fig. 6. It can be noted that complex shear modulus G^* gradually increased with the increase in frequency (Fig. 6(a)) at 64 °C. The G^* of SBR II emulsion residue was slightly lower than that of 0.5% WDC emulsion residue, indicating that the addition of low content of WDC had no significant effect on G^* at high temperatures. With the increase of

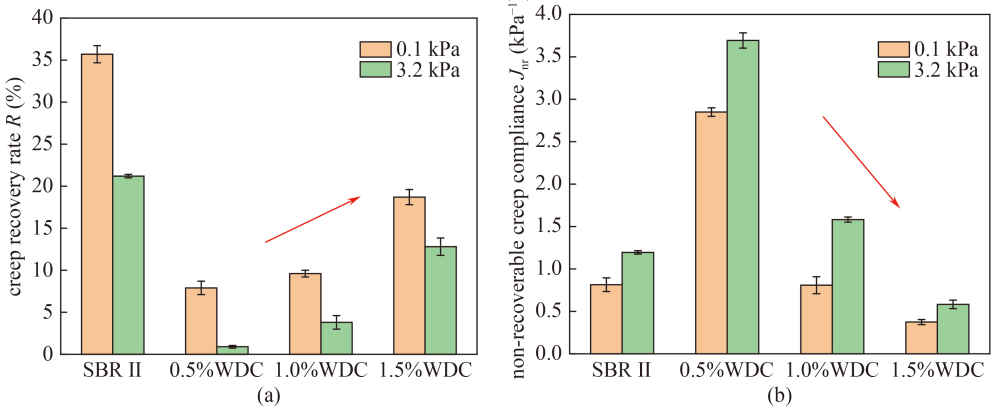

Fig. 5 J_{nr} and $R\%$ of various contents of WDC modified binder residues at 64 °C. (a) Creep recovery rate (R); (b) non-recoverable creep compliance J_{nr}.

WDC content, the G^* value increased, especially from 0.5% to 1.0%.

As for phase angle, the change of phase angle of modified emulsified asphalt binder with different WDC content showed different trends at different frequency ranges. The phase angle of 0.5% WDC and control binder reduced with frequency increase, while 1.0% WDC and 1.5%WDC followed the opposite trend. This trend can be explained by the effect of the formation of cross-linking by WDC. Because the morphology of WDC allows them to be bridged, and the high specific surface area and a large number of hydroxyl groups of nano cellulose can enhance this cross-linking [39]. However, the phase angle of 0.5% WDC was slightly higher than that of SBR II binder at over 3 rad/s. It can be concluded that low WDC content (below 1.0%) had no effect on the rheological properties of SBR emulsion residues.

3.5 The effect of nano-cellulose on aging resistance

Figure 7 shows the $G^*/\sin\delta$ values of virgin and RTFO-aged SBR I nano-cellulose emulsified asphalt residues at a temperature range from 58 to 70 °C. As expected, the rutting resistance of asphalt residue decreased rapidly with increased test temperatures. It can be explained that as the temperature rose, the asphalt binder transformed from elastomer to plasticity, the complex modulus decreased gradually, and the phase angle increased.

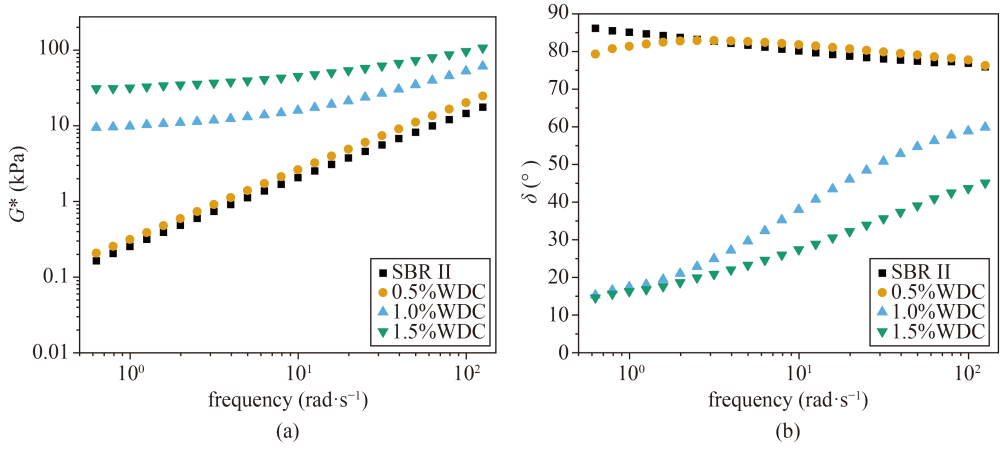

Fig. 6 G^* and phase angle value of various contents of WDC modified binder residues at 64 °C.

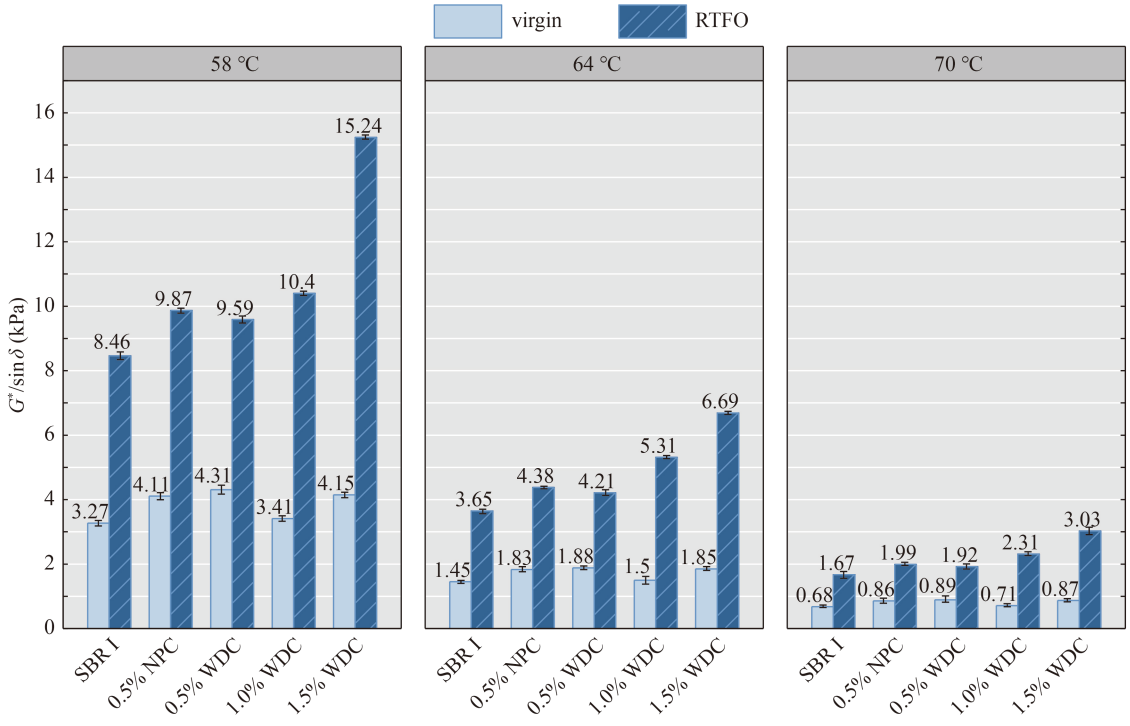

Fig. 7 $G^*/\sin\delta$ of SBR I asphalt residues with different nano-cellulose type and content.

After nano-cellulose was added, the $G^*/\sin\delta$ of virgin binder increased significantly regardless of nano-cellulose types, because the high specific surface area of nano-cellulose played a cross-linking role. In addition, the high-temperature performances of WDC modified asphalt binder were slightly better than the NPC modified asphalt binder at the same dosage, which can be attributed to the average length of two nano-celluloses.

For RTFO aged asphalt residue, the NPC modified binder indicated higher rutting factor than WDC modified binder at the content of 0.5% regardless of test temperatures. Moreover, with the increase of nano-cellulose dosage, the rutting factor of WDC modified binder increased gradually.

It can be seen from Fig. 8 that the *RAI* of WDC modified binder at three dosages indicated similar trends regardless of test temperature. The *RAI* of 0.5% nano-cellulose modified binder was less than that of the control binder regardless of nano-cellulose type, showing that 0.5% nano-cellulose had a positive effect on aging resistance. NPC modified binder had slightly better aging resistance than WDC modified binder at the same dosage. In addition, with the increase of WDC content, *RAI* significantly increased to about 200%, which was much higher than that of the SBR I binder residue. Therefore, the excessive addition of nano-cellulose cannot reduce the aging effect of asphalt binders, which can be attributed to the poor heat resistance and wear resistance of WDC [40]. At the same time, lignin in nano-cellulose may degrade during aging, which will be more obvious with the increase of nano-cellulose content [41].

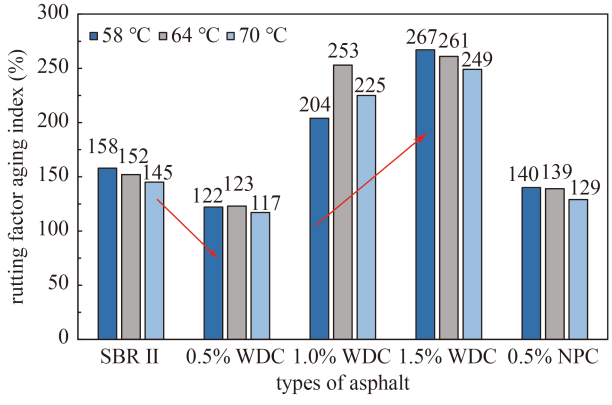

Fig. 8 *RAI* of nano-cellulose modified SBR I asphalt residue.

Furthermore, the statistical analysis in Table 3 shows that the effect of nano-cellulose on rutting factor is significant regardless of nano-cellulose type and dosage. The only exception is 1% WDC modified asphalt binder, for which no significant improvement of $G^*/\sin\delta$ was found after aging.

3.6 The effect of WDC content on fatigue performance

The fatigue factors $G^*\cdot\sin\delta$ of each asphalt residue are shown in Fig. 9. $G^*\cdot\sin\delta$ is related to the energy loss from the asphalt binder under repeated shear strain. The lower the $G^*\cdot\sin\delta$ of asphalt binder means less energy loss and the better fatigue resistance [42]. It can be found that as test temperature decreased, $G^*\cdot\sin\delta$ of all five asphalt residues gradually increased. After adding nano-cellulose, the fatigue factor of PAV aged asphalt significantly reduced, which meant that nano-cellulose could effectively improve the fatigue resistance of asphalt binder. This may be due to the high modulus and tensile strength of nano-cellulose, which can prolong the fatigue life [43].

NPC modified asphalt binder had better fatigue properties than WDC modified binder at the same nano-cellulose dosage. The fatigue factors of the control binder, 0.5% WDC modified emulsified asphalt, 1% WDC modified emulsified asphalt and 1.5% WDC modified emulsified asphalt at 25 °C were 2.70, 2.31, 1.64, and 1.94 kPa, respectively. As shown in Fig. 7, the fatigue factor showed a V-shape from 0.5% WDC to 1.5% WDC, indicating that 1.0% WDC had the best fatigue performance among all the binders, which can be attributed to the appropriate cross-linking structure in asphalt binder.

3.7 The effect of WDC content on low-temperature performance

The low-temperature performance of nano-cellulose modified emulsified asphalt binders was evaluated by BBR test. The test results are summarized in Table 4. It could be found that with the decrease of test temperature, the stiffness of asphalt binder increased, and the *m*-value decreased regardless of nano-cellulose type. This trend indicated that the relaxation capacity of asphalt binder decreased and asphalt binder became hardened and brittle

Table 3 Statistical Analysis of $G^*/\sin\delta$ of nano-cellulose modified asphalt residue

temperature (°C)	0.5% NPC		0.5% WDC		1% WDC		1.5% WDC	
	unaged	RTFO	unaged	RTFO	unaged	RTFO	unaged	RTFO
58	Y	Y	Y	Y	N	Y	Y	Y
64	Y	Y	Y	Y	N	Y	Y	Y
70	Y	Y	Y	Y	N	Y	Y	Y

Notes: Y represents that P-value < 0.05 (statistically different); N represents that P-value > 0.05 (no statistically different).

[44]. After adding nano-cellulose solution into SBR emulsified asphalt binder, the stiffness of nano-cellulose modified asphalt binder decreased, and the *m*-value increased, indicating that nano-cellulose could improve the low-temperature crack resistance. 1.0% WDC modified asphalt binder had the minimum stiffness modulus and the maximum *m*-value. Compared with 0.5% WDC modified binder, 0.5% NPC modified asphalt binder indicated slightly lower stiffness and higher *m*-value below –12 °C. This may be because WDC and NPC show different aspect ratio and morphology. Nano-cellulose with large aspect ratio and good network show better low-temperature crack resistance [43].

The differences between four nano-cellulose modified binders and SBR binder at various temperatures were analyzed. The results showed that adding 1.0% WDC reduced the stiffness modulus by 52%, 53%, and 46% at –6, –12, and –18 °C, respectively, and increased the *m*-value by 7%, 19%, and 35%, showing significant modification effect. For different nano-celluloses, the increased percentages in stiffness and the decrease percentage in *m*-value of NPC were lower than WDC at –6 °C.

The temperature at which the stiffness value of asphalt binder increases to more than 300 MPa is defined as stiffness based critical temperature ($T_{C,S}$), and the temperature at which the *m*-value of asphalt binder decreases below 0.3 is defined as *m*-value based critical temperature ($T_{C,m}$). Besides, the difference between $T_{C,S}$ and $T_{C,m}$ is the parameter named ΔT_c. Figure 10 summaries the calculated results of $T_{C,S}$, $T_{C,m}$, and ΔT_c of various asphalt binders.

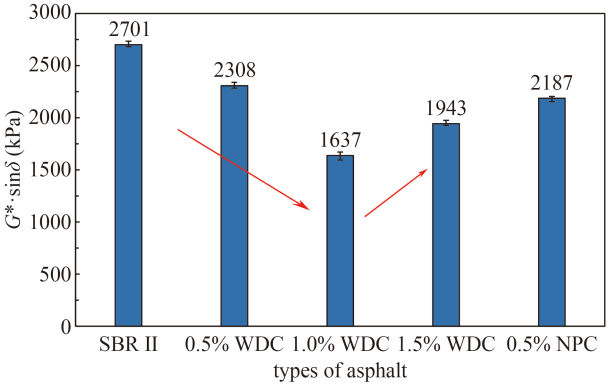

Fig. 9 $G^*\cdot\sin\delta$ of nano-cellulose modified SBR I asphalt residue at 25°C.

The $T_{C,S}$ of the control binder was around –14 °C. It can be seen from Fig. 10 that the $T_{C,S}$ of 0.5% NPC and 0.5% WDC modified asphalt binder were –18.48 and –17.12 °C, respectively. Therefore, the low-temperature performance of emulsified asphalt modified with 0.5% NPC was better for different nano-celluloses at the same dosage. In addition, the $T_{C,S}$ of 1.0% and 1.5% WDC modified emulsified asphalts were lower than –18 °C, and 1.0% WDC modified emulsified asphalt showed better low-temperature performance. Similarly, the $T_{C,m}$ of the control binder was around –13 °C. The $T_{C,m}$ value of 0.5% NPC modified binder was lower than 0.5% WDC modified binder. Moreover, the 1.0% WDC modified binder indicated the lowest $T_{C,m}$ among all the binders.

Based on the low-temperature cracking principle, a positive ΔT_c value indicates stiffness-controlled behavior [34], which means asphalt binders have a great relaxation property and a low risk of thermal cracking [45]. It can be found in Fig. 10 that all the asphalt binders had negative ΔT_c values and they would have a high risk of thermal cracking. Moreover, the ΔT_c value of 0.5% NPC modified asphalt binder was close to the warning line, which is –2.5 °C. Another noticeable trend was that with increase of nano-cellulose content, the ΔT_c values first decreased and then increased to –0.13 °C, which is the highest value for WDC modified binders. Based on these results, it can be concluded that the addition of nano-cellulose resulted in loss in the relaxation properties of asphalt binders.

3.8 ATR-FTIR

The ATR-FTIR spectrums of the fingerprint area for asphalt residues without aging are shown in Fig. 11. The peaks at around 700, 750, 800, and 850 cm^{-1} can be attributed to the deformation vibration of C-H under different substituents on the benzene ring. The peak at around 966 cm^{-1} can be attributed to the bending vibration of -CH=CH_2 in butadiene double bonds of SBR polymer. The C-H asymmetric deforming in CH_2 and CH_3, and the C-H symmetric deforming in CH_3 vibrations

Table 4 Results of low-temperature BBR test

asphalt type	–6 °C		–12 °C		–18 °C	
	stiffness (MPa)	*m*-value	stiffness (MPa)	*m*-value	stiffness (MPa)	*m*-value
SBR I	89.1	0.388	205.0	0.316	436	0.237
0.5% NPC	82.9	0.392	141.0	0.334	305	0.287
0.5% WDC	73.1	0.396	175.0	0.345	327	0.275
1.0% WDC	42.6	0.417	95.8	0.377	234	0.322
1.5% WDC	65.5	0.404	122.0	0.362	296	0.307

are at about 1460 and 1376 cm^{-1}, respectively. The peak area at 1030 cm^{-1} is S=O stretching vibrations, and the peak area at 1735 cm^{-1} are the carbonyl functions C=O. It can be seen from Fig.11 that no new functional groups were generated, and the absorption peak intensity of the functional groups was almost the same.

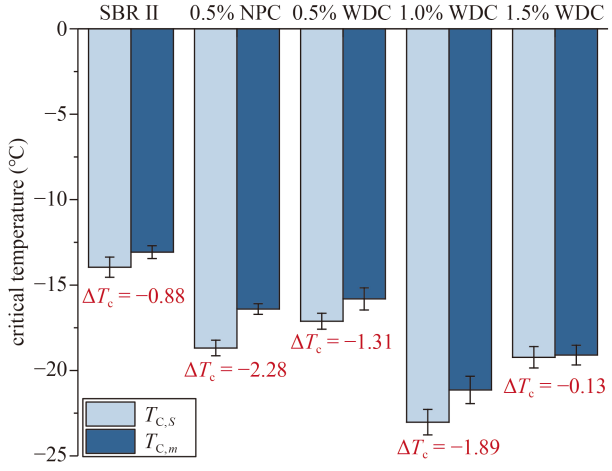

Fig. 10 $T_{C,S}$, $T_{C,m}$, and ΔT_c values of various asphalt binders.

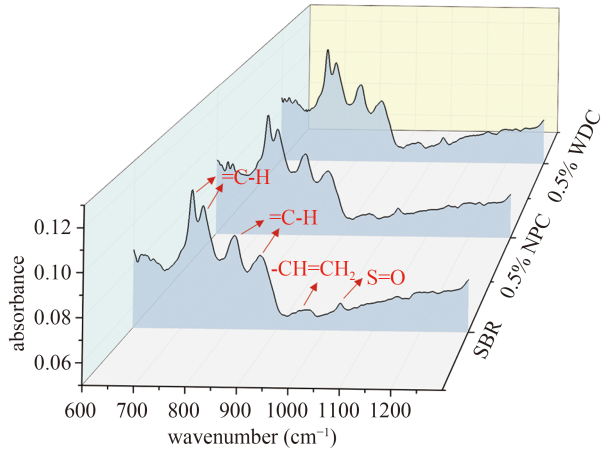

Fig. 11 Representative ATR-FTIR spectrum of various asphalt residues without aging.

For RTFO and PAV aged binder, the chemical index of aging related functional group (C=O and S=O) was used to determine the aging behavior of nano-cellulose modified binders [46] through semi-quantitative analysis. The functional groups at around 1460 and 1376 cm^{-1} were used to eliminate the influence of film thickness. The average value and standard error of C=O and S=O functional groups are presented in Figs. 12(a) and 12(b). It can be clearly found that the aging process had great influences on both S=O and C=O functional groups, regardless of nano-cellulose type. For short-term aging, the 0.5% NPC modified asphalt binder showed the highest improvement for both S=O and C=O, while the 0.5% WDC modified asphalt binder had a similar increment with a control binder. Previous research found that the intensity of C=O functional group in cellulose paper increased after fiber aging [47]. Therefore, it can be explained that both asphalt binder and NPC significantly aged during the RTFO procedure. After the long-term aging process, the 0.5% NPC modified asphalt binder indicated the lowest improvement of C=O and S=O functional groups among three binders. It can be inferred that NPC is more sensitive to short-term aging and generates carboxyl and carbonyl functional groups. These generated oxides may play a role in alleviating asphalt long-term aging.

4 Conclusions

This study prepared the TEMPO-oxidized NPC and WDC modified emulsified asphalt binders. The asphalt

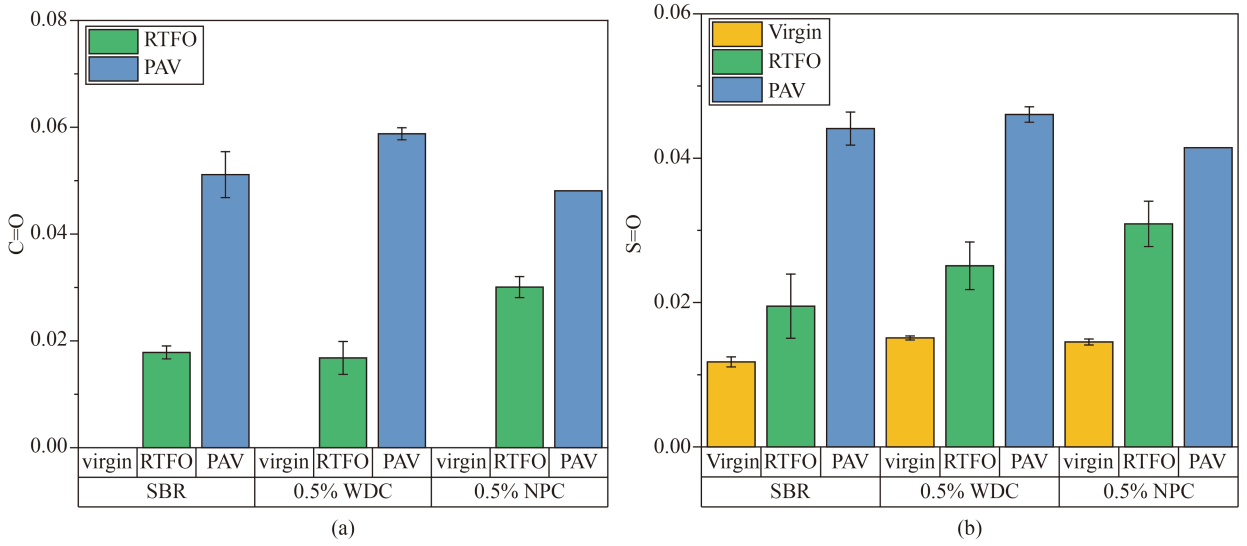

Fig. 12 Structural indices of aging related functional groups. (a) Carbonyl functional group C=O; (b) sulfoxide functional group S=O.

particle sizes and distributions were determined by microscopy and digital image analysis. The rheological properties at various temperatures were determined by DSR and BBR tests. Furthermore, the modification mechanism and aging behavior of nano-cellulose modified asphalt binder were analyzed by ATR-FTIR test. Based on the test results, the main conclusions that can be drawn are as follows.

1) The nano cellulose solution prepared by blending, ultrasonic stirring and centrifugal treatment can be effectively and evenly dispersed in emulsified asphalt binder; the average and maximum particle sizes of modified emulsified asphalt increase with the increase of nano-cellulose content.

2) Due to the cross-linking effect, the high-temperature performance and rutting resistance of modified emulsified asphalt were improved with the increase of nano-cellulose content. The addition of nano-cellulose had a negative effect on creep recovery R%, but high nano-cellulose content (>1%) had a positive effect on non-recoverable creep compliance J_{nr}.

3) For long-term aged binders, the NPC modified asphalt binder had better fatigue resistance and low-temperature performance than WDC modified binder at 0.5% dosage. Moreover, 1.0% WDC was the optimal option for improving fatigue and low-temperature performance. The addition of nano-cellulose led to a loss in the relaxation properties of asphalt binder, and 0.5% NPC modified asphalt binder had the lowest ΔT_c value.

4) 0.5% NPC modified asphalt binder generated more carbonyl functional groups during short-term aging, but it indicated the lowest improvement of C=O and S=O functional groups among three binders after long-term aging.

Acknowledgements This study was supported by the National Natural Science Foundation of China (Grant No. 51778478). The authors are also deeply grateful for the support from the Key Laboratory of Road and Traffic Engineering of Ministry of Education in Tongji University.

References

1. Hou X D, Xiao F P, Guo R, Xiang Q, Wang T, Wang J Y. Application of spectrophotometry on detecting asphalt content of emulsified asphalt. Journal of Cleaner Production, 2019, 215: 626−633
2. Wang C A, Wu Y L, Guo M Y, Chen M C. Development and applications of bitumen emulsion and its emulsifiers. Guangzhou Chemistry, 2006, 31(1): 54−60 (in Chinese)
3. Liu Y Y, Zhang Z Y, Tan L J, Xu Y, Wang C H, Liu P F, Yu H Y, Oeser M. Laboratory evaluation of emulsified asphalt reinforced with glass fiber treated with different methods. Journal of Cleaner Production, 2020, 274: 123116
4. Guan X. Research of performance for nano-ZnO/SBR modified asphalt mixture. Technology of Highway and Transport, 2021, 37(3): 28−33 (in Chinese)
5. Islam R M, Arafat S, Wasiuddin N M. Quantification of reduction in hydraulic conductivity and skid resistance caused by fog seal in low-volume roads. Transportation Research Record: Journal of the Transportation Research Board, 2017, 2657(1): 99−108
6. Xu L, Zhao Z F, Li X R, Yuan J, Zhou Q Y, Xiao F P. Cracking investigation on fog seal technology with waterborne acrylate and polyurethane as a clean modification approach. Journal of Cleaner Production, 2021, 329: 129751
7. Zhang H L, Su M M, Zhao S F, Zhang Y P, Zhang Z P. High and low temperature properties of nano-particles/polymer modified asphalt. Construction & Building Materials, 2016, 114: 323−332
8. Yan C Q, Lv Q, Zhang A A, Ai C F, Huang W D, Ren D Y. Modeling the modulus of bitumen/SBS composite at different temperatures based on kinetic models. Composites Science and Technology, 2022, 218: 109146
9. Yang J, Tighe S. A review of advances of nanotechnology in asphalt mixtures. Procedia: Social and Behavioral Sciences, 2013, 96: 1269−1276
10. Sun L, Xin X T, Wang H Y, Gu W J. Microscopic mechanismvof modified asphalt by multi-dimensional and multi-scale nanomaterial. Journal of the Chinese Ceramic Society, 2012, 40(10): 1437−1447
11. Li R Y, Xiao F P, Amirkhanian S, You Z P, Huang J. Developments of nano materials and technologies on asphalt materials—A review. Construction & Building Materials, 2017, 143: 633−648
12. He S J, Wang Y Q, Xi M M, Lin J, Xue Y, Zhang L Q. Prevention of oxide aging acceleration by nano-dispersed clay in styrene-butadiene rubber matrix. Polymer Degradation & Stability, 2013, 98(9): 1773−1779
13. Zhu C Z, Zhang H L, Xu G Q, Shi C J. Aging rheological characteristics of SBR modified asphalt with multi-dimensional nanomaterials. Construction & Building Materials, 2017, 151: 388−393
14. Zhang H L, Zhu C Z, Yu J Y, Shi C J, Zhang D M. Influence of surface modification on physical and ultraviolet aging resistance of bitumen containing inorganic nanoparticles. Construction & Building Materials, 2015, 98: 735−740
15. Huang B, Lu Q L, Tang L R. Research progress of nanocellulose manufacture and application. Journal of Forestry Engineering, 2016, 1(5): 1−9 (in Chinese)
16. Yao W R, Xu Q H. Research development of nano-cellulose preparation. Paper and Paper Making, 2014, 33(11): 49−55 (in Chinese)
17. Khattak M J, Khattab A, Rizvi H R, Zhang P F. The impact of carbon nano-fiber modification on asphalt binder rheology. Construction & Building Materials, 2012, 30: 257−264
18. Khattak M J, Khattab A, Rizvi H R. Characterization of carbon nano-fiber modified hot mix asphalt mixtures. Construction & Building Materials, 2013, 40: 738−745
19. Ghabchi R, Castro M P P. Effect of laboratory-produced cellulose nanofiber as an additive on performance of asphalt binders and mixes. Construction & Building Materials, 2021, 286: 122922
20. Jin J, Gao Y C, Wu Y R, Li R, Liu R H, Wei H, Qian G P, Zheng J L. Performance evaluation of surface-organic grafting on the

palygorskite nanofiber for the modification of asphalt. Construction & Building Materials, 2021, 268: 121072
21. Khattak M J, Khattab A, Zhang P F, Rizvi H R, Pesacreta T. Microstructure and fracture morphology of carbon nano-fiber modified asphalt and hot mix asphalt mixtures. Materials and Structures, 2013, 46(12): 2045−2057
22. Yang Q L, Li X L, Zhang L, Qian Y, Qi Y Z, Kouhestani H S, Shi X M, Gui X C, Wang D W, Zhong J. Performance evaluation of bitumen with a homogeneous dispersion of carbon nanotubes. Carbon, 2020, 158: 465−471
23. Li J, Yao S L, Xiao F P, Amirkhanian S N. Surface modification of ground tire rubber particles by cold plasma to improve compatibility in rubberised asphalt. International Journal of Pavement Engineering, 2022, 23(3): 651−662
24. Liu Z C. Reason for aggregation of nanoparticles in nano-materials and solutions. Value Engineering, 2017, 36(13): 157−158 (in Chinese)
25. Jamshidi A, Hasan M R M, Yao H, You Z P, Hamzah M O. Characterization of the rate of change of rheological properties of nano-modified asphalt. Construction & Building Materials, 2015, 98: 437−446
26. Khadivar A, Kavussi A. Rheological characteristics of SBR and NR polymer modified bitumen emulsions at average pavement temperatures. Construction & Building Materials, 2013, 47: 1099−1105
27. JTG E20-2011. Standard Test Methods of Bitumen and Bituminous Mixtures for Highway Engineering. Beijing: Ministry of Transport of the People's Republic of China, 2011 (in Chinese)
28. JTG F40-2004. Technical Specification for Construction of Highway Asphalt Pavement. Beijing: Ministry of Transport of the People's Republic of China, 2004 (in Chinese)
29. Saito T, Isogai A. Ion-exchange behavior of carboxylate groups in fibrous cellulose oxidized by the TEMPO-mediated system. Carbohydrate Polymers, 2005, 61(2): 183−190
30. Mathew A P, Oksman K, Karim Z, Liu P, Khan S A, Naseri N. Process scale up and characterization of wood cellulose nanocrystals hydrolysed using bioethanol pilot plant. Industrial Crops and Products, 2014, 58: 212−219
31. Bragd P L, van Bekkum H, Besemer A C. TEMPO-mediated oxidation of polysaccharides: survey of methods and applications. Topics in Catalysis, 2004, 27(1): 49−66
32. Dai S L, Wang Y, Zhang J Y, Zhao Y W, Xiao F P, Liu D P, Wang T R, Huang J. Wood-derived nanopaper dielectrics for organic synaptic transistors. ACS Applied Materials & Interfaces, 2018, 10(46): 39983−39991
33. AASHTO T-315. Standard Method of Test for Determining the Rheological Properties of Asphalt Binder Using a Dynamic Shear Rheometer (DSR). Washington, D.C.: American Association of State Highway and Transportation Officials (AASHTO), 2019
34. Elwardany M, Planche J P, King G. Universal and practical approach to evaluate asphalt binder resistance to thermally-induced surface damage. Construction & Building Materials, 2020, 255: 119331
35. Anderson R M, King G N, Hanson D I, Blankenship P B. Evaluation of the relationship between asphalt binder properties and non-load related cracking. Electronic Journal of the Association of Asphalt Paving Technologists, 2011, 80: 615−664
36. Hou X D, Lv S T, Chen Z, Xiao F P. Applications of Fourier transform infrared spectroscopy technologies on asphalt materials. Measurement, 2018, 121: 304−316
37. Amirkhanian A N, Xiao F P, Amirkhanian S N. Characterization of unaged asphalt binder modified with carbon nano particles. International Journal of Pavement Research and Technology, 2011, 4(5): 281−286
38. Wang S Q, Wei C, Gong Y Y, Lv J, Yu C B, Yu J H. Cellulose nanofiber-assisted dispersion of cellulose nanocrystals@polyaniline in water and its conductive films. RSC Advances, 2016, 6(12): 10168−10174
39. Souza L O, Cordazzo M, Souza L M S, Tonoli G, Silva F A, Mechtcherine V. Investigation of dispersion methodologies of microcrystalline and nano-fibrillated cellulose on cement pastes. Cement and Concrete Composites, 2022, 126: 104351
40. Tian H, Zeng M L, Wu C F, Xia Y, Zhu Y F. Effect of glass fiber and plant fiber on high temperature performance of unaged and aged asphalt mortar. Highway Engineering, 2008, 33(4): 37−41 (in Chinese)
41. Yuan B N, Guo M H, Huang Z H, Naik N, Hu Q, Guo Z H. A UV-shielding and hydrophobic graphitic carbon nitride nanosheets/cellulose nanofibril (gCNNS/CNF) transparent coating on wood surface for weathering resistance. Progress in Organic Coatings, 2021, 159: 106440
42. Cheng H L, Sun L J, Wang Y H, Chen X Y. Effects of actual loading waveforms on the fatigue behaviours of asphalt mixtures. International Journal of Fatigue, 2021, 151: 106386
43. Castro M P P. Effects of cellulose nano-fiber as an additive on performance of asphalt binders and mixes. Thesis for the Master's Degree. Vermillion, SD: South Dakota State University, 2020
44. Hou X D, Xiao F P, Wang J Y, Amirkhanian S. Identification of asphalt aging characterization by spectrophotometry technique. Fuel, 2018, 226: 230−239
45. Zhang H Y, Xu G, Chen X H, Wang R, Shen K R. Effect of long-term laboratory aging on rheological properties and cracking resistance of polymer-modified asphalt binders at intermediate and low temperature range. Construction & Building Materials, 2019, 226: 767−777
46. Wang J Y, Wang T, Hou X D, Xiao F P. Modelling of rheological and chemical properties of asphalt binder considering SARA fraction. Fuel, 2019, 238: 320−330
47. Chen S, Xu H, He X Y, Su Y, Zhang B, Liu Q. Oil-grinded recycled kapok fiber as a bio-packing for eco-friendly modified asphalt and its aging resistance behavior. Construction & Building Materials, 2022, 320: 126293